An Image-Based Model of Atrial Muscular Architecture
Effects of Structural Anisotropy on Electrical Activation

Jichao Zhao, PhD; Timothy D. Butters, PhD Candidate; Henggui Zhang, PhD; Andrew J. Pullan, PhD†; Ian J. LeGrice, MBChB, PhD; Gregory B. Sands, PhD; Bruce H. Smaill, PhD

Background—Computer models that capture key features of the heterogeneous myofiber architecture of right and left atria and interatrial septum provide a means of investigating the mechanisms responsible for atrial arrhythmia. The data necessary to implement such models have not previously been available. The aims of this study were to characterize surface geometry and myofiber architecture throughout the atrial chambers and to investigate the effects of this structure on atrial activation.

Methods and Results—Atrial surface geometry and myofiber orientations were reconstructed in 3D at $50\times50\times50$-μm^3 resolution from serial images acquired throughout the sheep atrial chambers. Myofiber orientations were determined by Eigen-analysis of the structure tensor. These data have been incorporated into an anatomic model that provides the first quantitative representation of myofiber architecture throughout the atrial chambers. By simulating activation on this 3D structure, we have confirmed the roles of specialized myofiber tracts such as the crista terminalis, pectinate muscles, and the Bachman bundle on the spread of activation from the sinus node. We also demonstrate how the complex myocyte arrangement in the posterior left atrium contributes to activation time dispersion adjacent to the pulmonary veins and increased vulnerability to rhythm disturbance generated by ectopic stimuli originating in the pulmonary vein sleeves.

Conclusions—We have developed a structurally detailed, image-based model of atrial anatomy that provides deeper understanding of the role that myocyte architecture plays in normal and abnormal atrial electric function. **(*Circ Arrhythm Electrophysiol*. 2012;5:361-370.)**

Key Words: atrial fibrillation ■ atrial myoarchitecture ■ fiber orientation ■ computer model ■ electric simulation

Atrial arrhythmias are the most common heart rhythm disturbances. Chronic atrial fibrillation (AF) is prevalent in the elderly, increases the risk of stroke, and contributes to mortality in congestive heart failure. There is a strong association between these arrhythmias and the structural remodeling of the atrial chambers that occurs with aging and heart disease.[1] However, despite extensive anatomic and experimental research, the linkage between atrial structure and electric function is not completely understood in the normal heart, let alone in structural heart disease.

Clinical Perspective on p 370

Computer models provide a promising framework for investigating factors that contribute to the initiation and maintenance of reentrant atrial arrhythmias. This view has motivated the development of numerous models of atrial electric function over the past decade.[2–6] Several of these have incorporated accurate representations of 3D atrial surface geometry[2,4] and regional differences in atrial electric properties,[4,5] but none has included detailed descriptions of muscular architecture throughout the atria. Instead, most have assumed that the electric properties of atrial myocardium are isotropic[3] or have incorporated prescribed local anisotropy to account for the role of specialized conduction tracts such as the Bachman bundle (BB) and the pectinate muscles (PMs).[2,4,5]

Macroscopic descriptions of atrial muscle fiber organization have been reported in a number of previous studies.[7,8] High resolution 3D reconstructions of the sinoatrial node (SAN),[9] atrioventricular node (AVN),[10] and right atrial appendage (RAA)[6] have also been presented and it is possible to infer myocyte orientation in each of these. However, intramural myofiber architecture has not been systematically quantified in the atria as has been done for right and left ventricles, using histological techniques[11] and diffusion tensor MRI (DTMRI).[12]

In the current study, we present for the first time an image-based, 3D anatomic model of the sheep atria that

Received September 22, 2011; accepted February 27, 2012.

From Auckland Bioengineering Institute (J.Z., A.J.P., I.J.L., G.B.S., B.H.S.), Engineering Science (A.J.P.), and Physiology (I.J.L., B.H.S.), University of Auckland, Auckland, New Zealand; and the School of Physics and Astronomy, University of Manchester, Manchester, United Kingdom (T.D.B., H.Z.).

†Deceased.

The online-only Data Supplement is available at http://circep.ahajournals.org/lookup/suppl/doi:10.1161/CIRCEP.111.967950/-/DC1.

Correspondence to Jichao Zhao, PhD, Auckland Bioengineering Institute, University of Auckland, Auckland, New Zealand. E-mail j.zhao@auckland.ac.nz

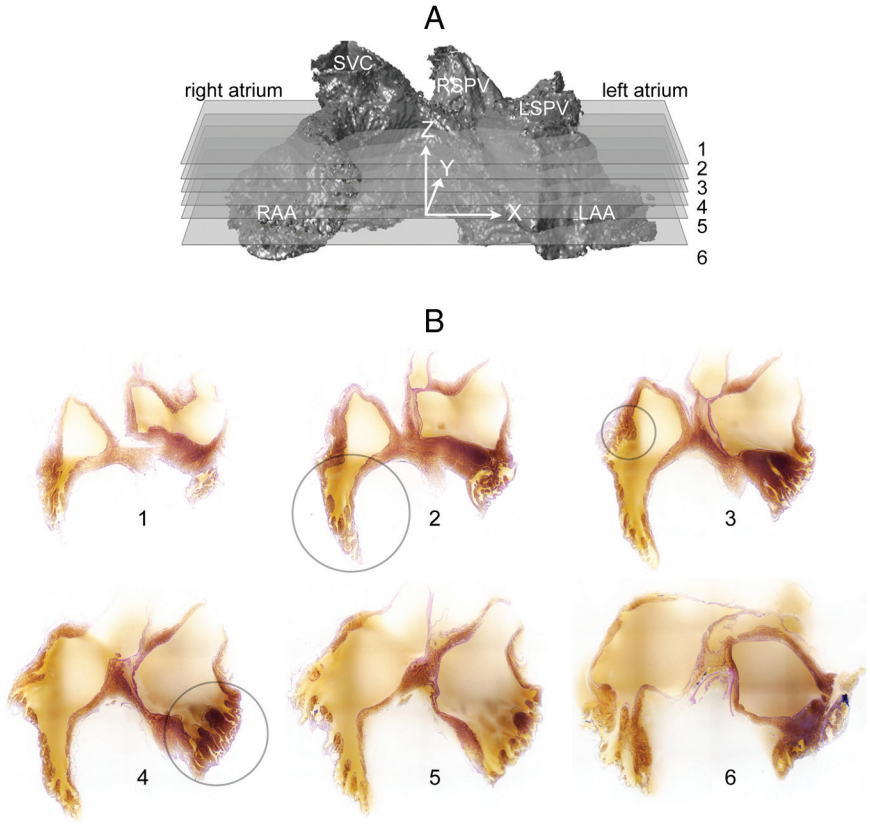

Figure 1. Volume image of the sheep atria acquired by serial surface imaging. **A**, Anterior view of 3D reconstruction of epicardial surface. The superior vena cava (SVC), right superior pulmonary vein (RSPV), left superior pulmonary vein (LSPV), right atrial appendage (RAA), and left atrial appendage (LAA) are indicated. **B**, Representative 2D image montages at **1** to **6**: Z=20 mm, 17.5 mm, 15 mm, 12.5 mm, 10 mm, and 5.4 mm, respectively, where the distances were measured from the bottom of stack. Section locations indicated by semitransparent planes in **A**. Approximate boundaries of RAA and LAA are indicated in **2** and **4**, respectively. The complex structure of the pectinate muscles (PMs) is evident in both. The **circle** in **3** is centered on the crista terminalis.

includes comprehensive descriptions of surface geometry and myocyte organization throughout the atrial chambers. We have used these data to investigate the extent to which myofiber architecture affects the spread of atrial electric activation, with particular emphasis on the posterior left atrium (PLA).

Methods

This study was approved by the Animal Ethics Committee of The University of Auckland and conforms to the *Guide for the Care and Use of Laboratory Animals* (NIH publication No. 85–23). More detailed information on the methods used is provided in the online-only Data Supplement.

Image Acquisition and Processing

The atria from a normal sheep heart were fixed at physiological filling pressure and embedded in paraffin wax. Serial surface images were acquired throughout this volume as follows. The upper surface was planed using an Ultramiller, etched to a depth of ≈2 μm, stained with Toluidine blue, and imaged at 8.33-μm pixel resolution using a digital camera equipped with a macro lens. This process was repeated in 50-μm steps. A suite of image processing tools (see online-only Data Supplement Figure I) was used (1) to smooth internal structures and extract tissue boundaries in individual image sections and (2) to smooth the volume image. From these serial images, the atria were reconstructed in 3D with $50\times50\times50$-μm^3 voxel dimensions and are represented in Figure 1, together with representative image sections, before segmentation.

Atrial Myofiber Orientation

Eigen-analysis of the structure tensor constructed from the image volume was used to estimate local myofiber orientation (for detail, see the online-only Data Supplement). Atrial myofiber orientations are initially defined with respect to the imaging coordinate system but are also referred to local coordinate systems where appropriate. For the imaging coordinate system (X, Y, Z), the X-Y plane is near parallel to the atrioventricular (AV) valve plane, whereas the Z-axis lies within the interatrial septum. We define longitudinal as parallel to the Z direction. Atrial myofiber orientation is specified by defining 2 angles: the inclination angle α is the projection of the fiber vector onto a plane parallel to the local epicardial surface, measured with respect to the horizontal, whereas the transverse angle β is the projection onto the horizontal plane, with respect to the surface tangent plane (see online-only Data Supplement Figure III).

Modeling Atrial Activation

The spread of atrial electric activation was simulated by solving the monodomain reaction-diffusion equation on a 3D voxel-based finite difference grid ($100\times100\times100$-μm^3 resolution), using the Fenton-Karma activation model.[13] Solutions for isotropic electric properties (conductivity=2.4 mS) and axially anisotropic electric properties (axial and transverse conductivities 9.0 mS and 0.9 mS, respectively) are compared. These values were selected to minimize the difference in predicted activation spread for isotropic and anisotropic cases in regions where myofiber architecture is disordered.

Results

Atrial Myofiber Architecture

Myofiber arrangement, visualized using fiber-tracking techniques, is rendered on an anterosuperior view of the atria in Figure 2A. This representation is dominated by the subepicardial myofiber organization, but the circumferential orientation of myofibers at the base of the superior vena cava (SVC) and around the pulmonary veins (PV) is evident. Also clear is the BB, which originates near the anterior junction of the SVC and right atrium (RA) and runs leftward parallel to the X-Y plane across the interatrial groove to the left atrium (LA). This fiber tract continues circumferentially (with re-

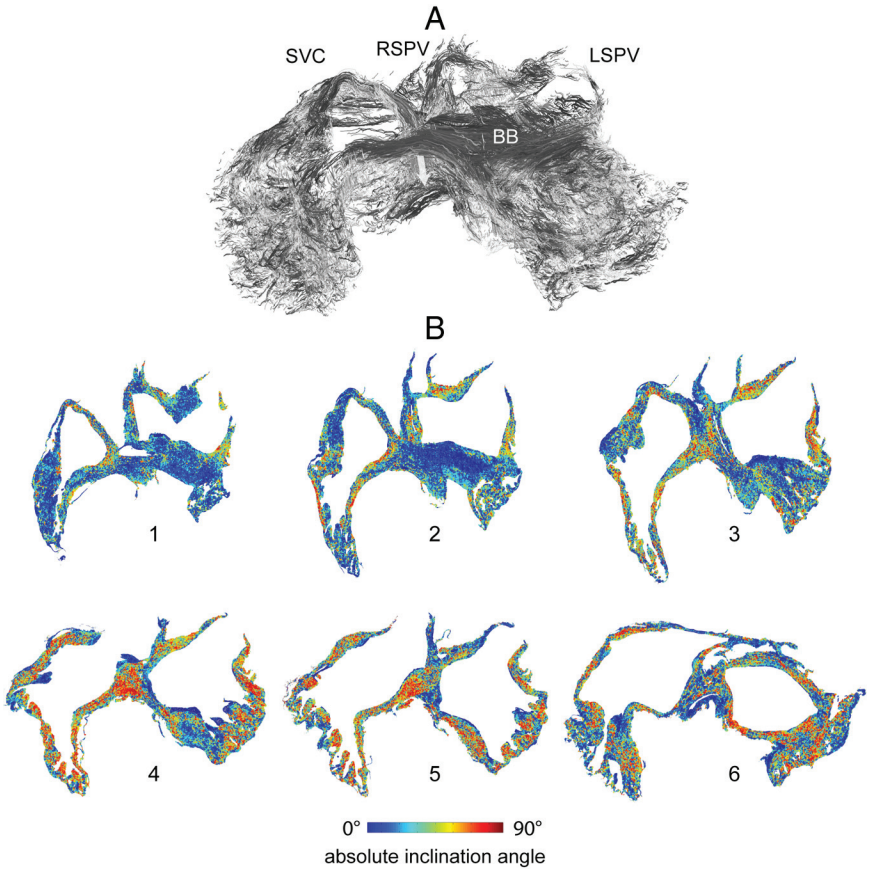

Figure 2. Atrial surface geometry and intramural myofiber orientation. **A**, Anterosuperior view of 3D atrial myofiber tracts. Gray-scale intensity selected to emphasize tract orientation. **Arrow** indicates the orientation of fibers in the interatrial groove immediately behind the Bachman bundle (BB). **B**, Myofiber inclination in representative sections **1** to **6**, as indicated in Figure 1. Color spectrum represents absolute myofiber inclination angle with respect to the *X-Y* plane. SVC indicates superior vena cava; RSPV, right superior pulmonary vein; and LSPV, left superior pulmonary vein.

spect to the *Z*-axis) across the top of the LA but gives rise to 2 separate branches. One tracks downward in the LA wall adjacent to the interatrial groove and the other passes along the anterior edge of the left atrial appendage (LAA). Finally, longitudinal myofibers can also be seen immediately below the BB in the interatrial groove between the RA and the LA (see arrow in Figure 2A).

Figure 2B presents myofiber inclination angles mapped onto 6 representative horizontal sections through the atria (see Figure 1B). There are distinct regions of uniformly aligned myofibers throughout the atria. For instance, the BB merges with an extensive band of fibers parallel to it that form the inner half of the anterior LA wall in Figure 2B (2), whereas a second band tracks downward (with respect to the *X-Y* plane) in the outer LA wall. The orientation of myofibers in much of the interatrial septum and also the septo-pulmonary bundle (SPB) between the right and left inferior PVs (RIPV, LIPV) in the posterior LA wall is uniformly longitudinal. Highly organized tracts such as the crista terminalis (CT) and PMs are also apparent on the endocardial surfaces of the RA wall and the atrial appendages. However, there is no evidence of uniform transmural myofiber rotation (as seen in the ventricles).

Higher-resolution fiber tracking has been used to investigate the microscopic organization of muscle bundles characterized by a high level of myocyte alignment. Typical results are presented in Figure 3. The architecture of a segment from the upper surface of the RAA (7.5×17.5×4 mm; location indicated in Figure 3A) is shown in Figure 3B. Three orthogonal sections indicate the topology of large PM bundles close to their origin along the CT. Fiber pathways are superimposed on these sections and color-coded for inclination angle. As expected, myofibers are strongly aligned with the long axis of the PM bundles. On the other hand, myofiber orientations in the thin atrial wall differ dramatically from PM direction and vary with location. Also, the orientation of myocytes in the large PM bundles is markedly different from those in the CT from which they originate. In Figure 3D through 3F, myocyte organization in the BB is visualized in an anterosuperior segment close to the point at which the BB branches on the left side of the interatrial groove (25×15×7.5 mm; see Figure 3D for location). The ordered myofiber alignment in the BB is clear when fiber tracks are superimposed on orthogonal sections reconstructed within the segment. The BB bifurcates immediately to the left of the interatrial groove; the main stem of the BB continues, while the branch eventually tracks downward toward the *AV* valve plane.

In Figure 4, we focus on the PLA, with specific emphasis on myofiber architecture at the junction of the PVs and LA. Atrial myocytes in the PLA have an ordered arrangement and wrap circumferentially around the PVs adjacent to the veno-atrial junctions. However, there are abrupt changes in geometry and myofiber orientation in the PV sleeves as the veno-atrial junctions are approached. This is evident in Figure 4D, where fiber tracks are rendered on a segment from the right side of the LIPV that also traverses the posterior SPB. The sleeve is thin-walled distal to the veno-atrial junction

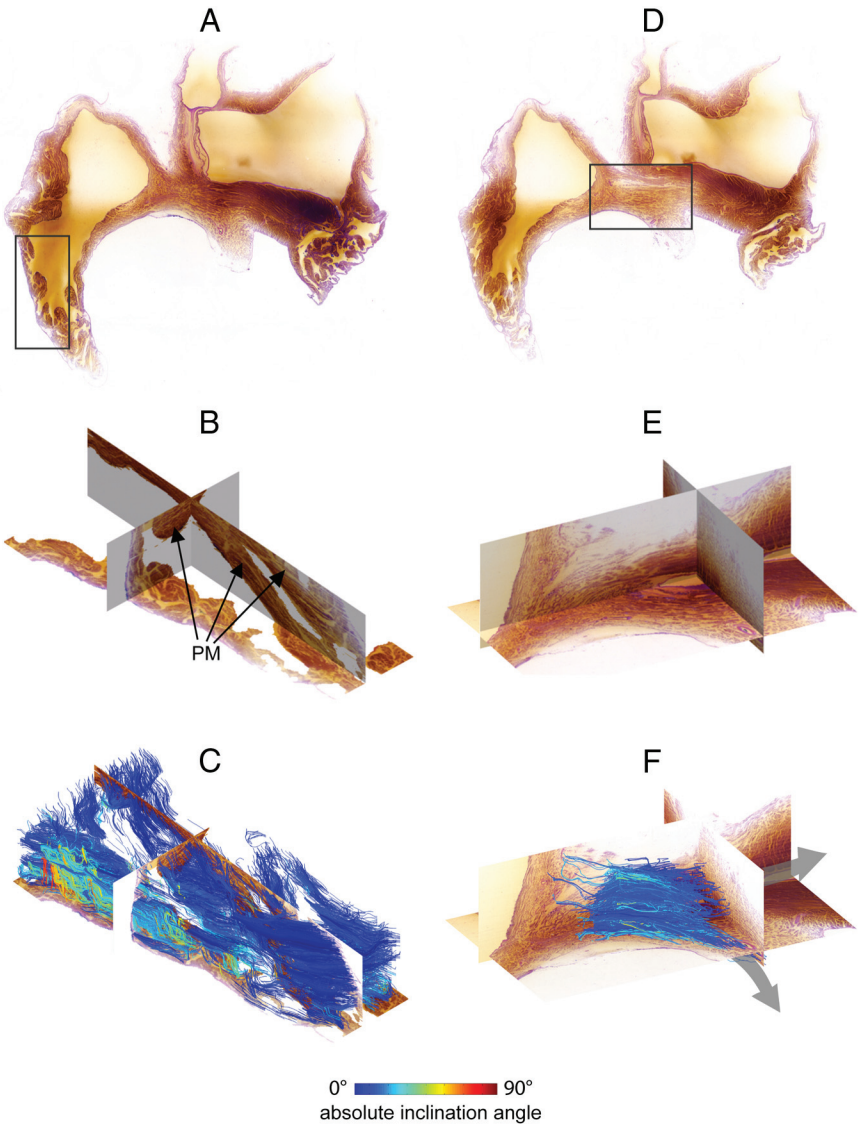

Figure 3. Myofiber architecture in image segments from the right atrial appendage (RAA) and Bachman bundle (BB). **A**, Location of RAA segment (7.5×17.5×4 mm, centered at $Z=17$ mm; see Figure 1). **B**, Orthogonal image planes on image segment, with **C**, high-resolution fiber tracts rendered on them. **D**, Location of segment from the BB (25×15×7.5 mm, centered at $Z=18.8$ mm; see Figure 1). **E**, Orthogonal image planes from image segment, with **F**, high-resolution fiber tracts rendered on them. Color spectrum in **C** and **F** represents absolute myofiber inclination angle with respect to the *X-Y* plane. PM indicates pectinate muscle.

with myofibers predominantly aligned with the *PV* axis. Sleeve thickness increases abruptly at the veno-atrial junction (from ≈1 mm to ≈4 mm in Figure 4C) and myofibers rotate sharply through ≈90°.

Effects of Atrial Myofiber Architecture and Geometry on Electric Activation

To investigate the effects of myofiber architecture on atrial electric activation, we simulated activation spread on the 3D atrial model with isotropic and anisotropic electric properties. The former gives rise to a uniform conduction velocity (CV) of ≈0.75 m/s, whereas the latter produces CVs of ≈1.13 m/s along the fiber direction and ≈0.63 m/s cross-fiber in the RAA segment, where myofibers are uniformly oriented. For regions with heterogeneous myofiber organization, there was very little difference in the activation spread predicted with isotropic and anisotropic electric properties (see online-only Data Supplement Figure V).

In Figure 5, we compare the spread of electric activation from a stimulus site at or near the SAN with isotropic and anisotropic electric properties. Activation spreads uniformly from this site in the isotopic case and is completed ≈116 ms after stimulation. The activation sequence is qualitatively different in the anisotropic case, where preferential propagation pathways are evident in the epicardial activation patterns, and activation was completed within 98 ms. Specific differences include rapid spread from the SAN across the superior RA into the RAA (within 40 ms) and from the RA to the LA, with much of the superior LA activated within 40 to 50 ms. On the other hand, propagation from top to bottom of the atria (particularly the LA) was marginally slower with anisotropic than isotropic electric properties. The role of the CT and PM in the activation of the RAA is indicated by the fact that epicardial activation reflects PM structure. The effects of preferential axial conduction in the BB and to a lesser extent the functional extension of the BB that extends across the anterior surface of the LA are also clear. Finally, activation spreads more rapidly across the LA roof and around the PVs in the anisotropic case.

Further detail on the intramural spread of atrial electric activation is provided in Figure 6, where activation isochrones are superimposed on the 6 representative horizontal

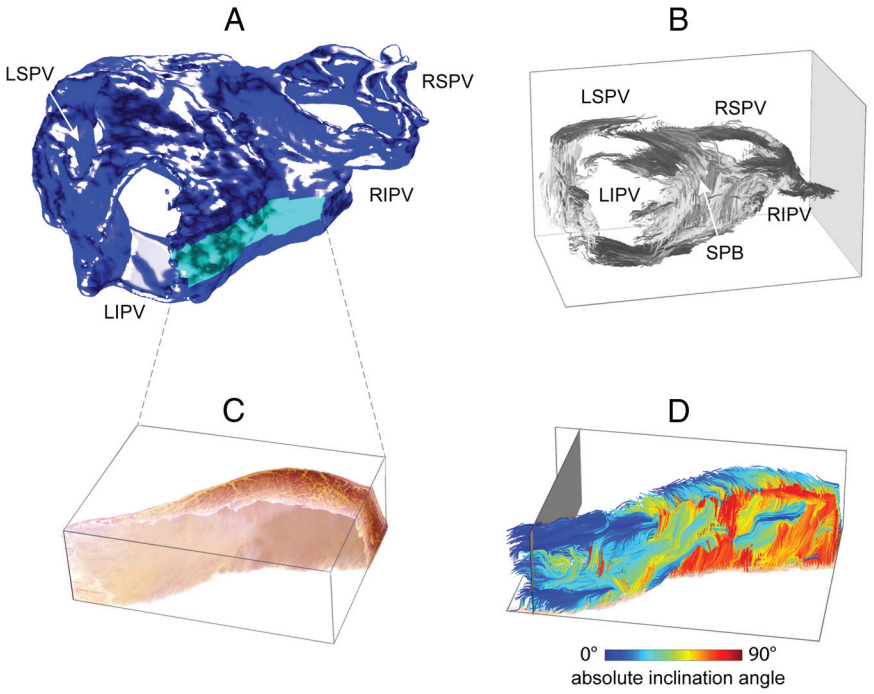

Figure 4. Myofiber architecture in posterior left atrium (LA). **A**, Three-dimensional reconstruction of posterior LA including pulmonary veins. **B**, Three-dimensional fiber tracks in posterior LA rendered on same posterior view. Gray-scale intensity is selected to emphasize tract orientation and the superior pulmonary bundle (SPB) is indicated. **C**, Three-dimensional reconstruction of image segment digitally sectioned from the left inferior pulmonary vein (LIPV) adjacent atrial wall as shown in **A**. The endocardial (lumenal) side is innermost. **D**, High-resolution fiber tracking for subvolume in **C**. LSPV indicates left superior pulmonary vein; RSPV, right superior pulmonary vein; and RIPV, right inferior pulmonary vein. Color spectrum as indicated in Figure 3.

sections in Figure 1B. Activation of endocardial and epicardial surfaces of the atria was relatively synchronous for both isotropic and regionally anisotropic cases. However, the effects in the latter of preferential conduction pathways are evident in the nonuniform distribution of intramural isochrones in associated sections. In the RAA and LAA, contours spread from endocardial to epicardial surfaces in isotropic and anisotropic models. This progression indicates that activation of the atrial appendices is driven by the PMs in both cases but to a much greater extent in the anisotropic model.

The effects of myofiber anisotropy on the spread of atrial electric activation are most marked in the PLA and are shown at higher resolution in Figure 7. In the isotropic case, activation spreads uniformly around the junctions of the right PVs with near synchronous depolarization of the left PV junctions and the lateral margin of the PLA. In comparison, the ordered arrangement of myofibers in the PLA produces strikingly different activation patterns for the anisotropic case. Activation spreads rapidly along the antero-superior margin of the LA (via the BB and its extensions) and across the LA roof and posterior wall between the right and left PVs

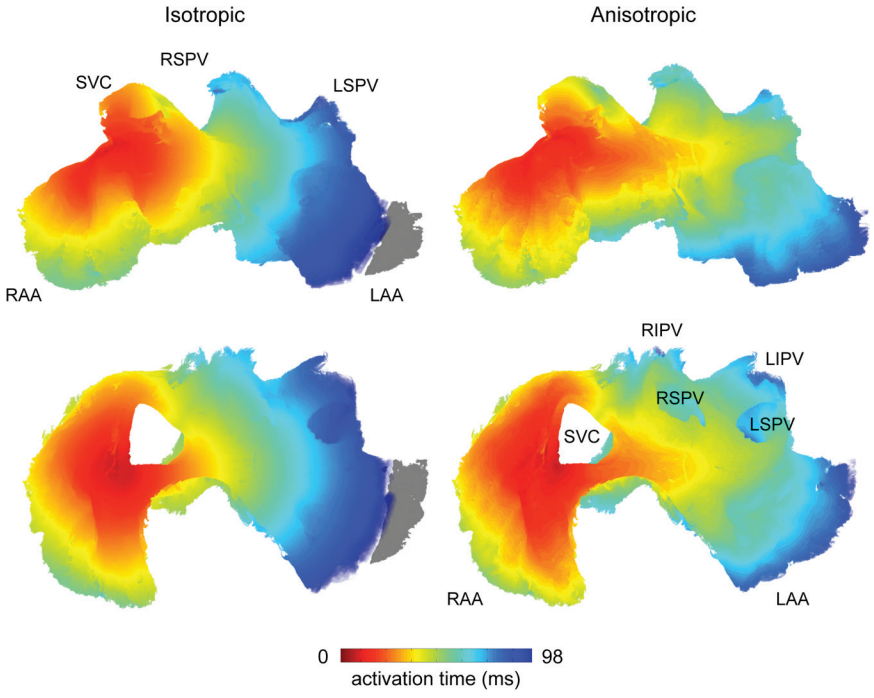

Figure 5. Comparison of effects of isotropic and anisotropic electric properties on epicardial spread of electric activation simulated on 3D atrial model incorporating myofiber orientation data. Activation isochrones are rendered on anterosuperior and superior views of the atria in **upper** and **lower** panels, respectively. Activation time key for the color map (indicated) same for both. Region in isotropic model not yet activated at 98 ms is indicated in gray. SVC indicates superior vena cava; RSPV, right superior pulmonary vein; LSPV, left superior pulmonary vein; RAA, right atrial appendage; LAA, left atrial appendage; RIPV, right inferior pulmonary vein; and LIPV, left inferior pulmonary vein.

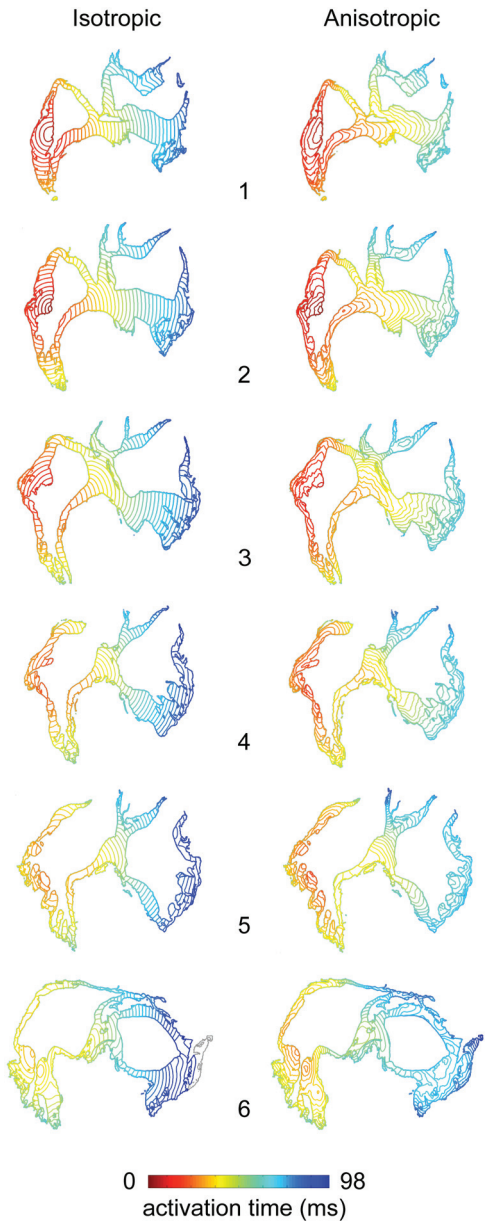

Figure 6. Comparison of effects of isotropic and anisotropic electric properties on intramural spread of electric activation simulated on 3D anatomic model incorporating myofiber orientation data. Activation isochrones mapped on representative sections **1** to **6**, as indicated in Figure 1. Activation time key for the color map (indicated), same for both. Region in isotropic model not yet activated at 98 ms is indicated in gray.

(via the SPB). This results in substantial activation time dispersion in the vicinity of the PV junctions and, in particular, adjacent to the LIPV. Latest activation in the lateral edge of the PLA in the anisotropic case occurs in the distal sleeve of the LIPV.

The effects of structural anisotropy on the spread of electric activation from ectopic stimuli in the PLA were investigated by imposing S_2 stimuli adjacent to the PV sleeves after S_1 stimulation near the SAN. The coupling interval was set to the minimum necessary to evoke propagated electric activity (for further detail, see the online-only Data Supplement). Compared with isotropic electric properties, successful propagation was achieved at shorter coupling intervals in the anisotropic case (around 6 ms earlier during repolarization); however, there were substantial initial time delays. The time for activation to reach a line along the SPB, midway between left and right PVs, was 26 ± 10 ms greater for anisotropic than for isotropic electric properties. Initial activation slowing was observed at all 4 PVs, but the range was greatest for the left PVs. A typical example is given in Figure 8C, where activation initially spreads very slowly around the LSPV junction in the myofiber direction but blocks elsewhere (see lines at 40 ms). Of particular interest is the conduction block at this time from the veno-atrial junction into the SPB, transverse to the fiber direction. Tortuous propagation upward and into the SPB, as well as around the LIPV, at 80 ms seeds subsequent coordinated activation of the LA. With isotropic electric properties, activation from the same site was more difficult to achieve initially but spread uniformly across the LA roof and around the left PVs (see Figure 8D), reaching the midline of the SPB $\approx$44 ms earlier.

Discussion

The spread of electric activation through the atrial chambers of the heart is determined by their geometry and muscular architecture.[8] More comprehensive understanding of the effects of tissue structure on electric function is necessary for effective nonpharmacologic treatment of atrial arrhythmias. In this study, we have developed an image-based model of 3D atrial anatomy, the first as far as we are aware to incorporate a realistic description of myofiber architecture as well as atrial surface geometry. Simulations of electric activation on this structure indicate that the organization of atrial muscle bundles gives rise to significant activation time dispersion in regions such as the PLA. The results of this work support the position taken by Ho et al[8] (2009), who argued that the heterogeneous myoarchitecture of RA and LA and interatrial septum must be taken into account in computer models that seek to investigate mechanisms of atrial arrhythmia.

Computer models are increasingly being used to investigate mechanisms underlying atrial arrhythmias. These include 2D models,[14] monolayer models,[3] models based on simplified morphology,[15] and 3D models.[2,5] Progressively, computer models have incorporated increased geometric complexity (derived from magnetic resonance or computed tomography image data sets) and differing activation kinetics for different atrial regions. On the other hand, fiber orientation and anisotropic electric properties have to date been assigned manually to prominent fiber bundles only, such as the BB and the right atrial PMs. Our model of atrial structure advances previous work in this area because it captures key features of myofiber architecture throughout the atrial chambers.

Atrial Myofiber Architecture

Systematic investigations of myofiber arrangement in left and right ventricles, using serial histological measurements[11] and DTMRI,[12] have demonstrated uniform transmural myofiber rotation that varies predictably between regions and is replicated in different species. Comparable, quantitative data have not been available for the atria. The muscular architecture of

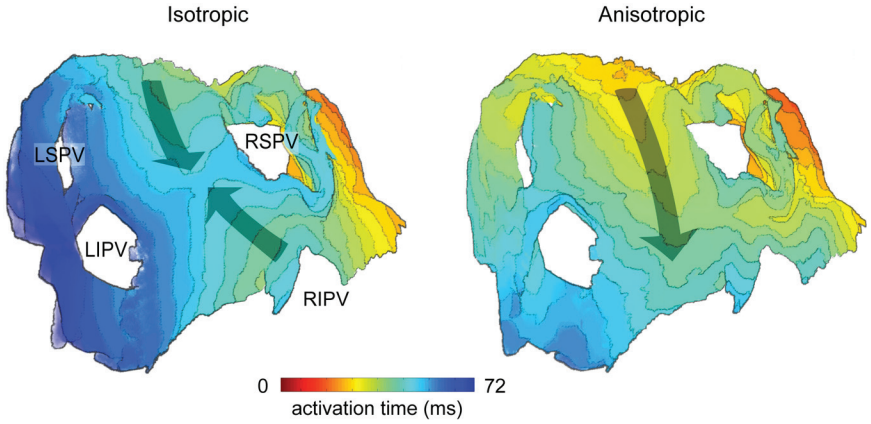

Figure 7. Comparison of effects of isotropic and anisotropic electric properties on epicardial electric activation in the posterior left atrium (PLA). Activation time isochrones rendered on posterior view of PLA (see Figure 4A). **Arrows** indicate the spread of activation across the left atrium roof. Color spectrum indicates time from first activation. RSPV indicates right superior pulmonary vein; LSPV, left superior pulmonary vein; RIPV, right inferior pulmonary vein; and LIPV, left inferior pulmonary vein. Isochrone separation, 3 ms.

the atria varies across multiple length scales and DTMRI lacks the spatial resolution to capture the complex fibrous architecture of the atrial wall fully. Specialized structures such as the SAN and AVN have been reconstructed in 3D at high spatial resolution 3D,[9,10] using serial microscopy. However, our understanding of atrial fiber arrangement and preferential conduction pathways is based on careful anatomic studies by Ho, Anderson, and coworkers,[7,8] using dissection, macrophotography, and visual tracing of fiber tracts.

We have estimated myofiber orientation throughout the atria from the 3D structure tensor constructed from the atrial image volume. This well-established image processing technique[16] uses methods that are near identical to those used in DTMRI. The intramural fiber orientations obtained in the sheep atria generally match the picture of muscular architecture built up by systematic dissection of human atria.[7,8] Myocyte arrangement in the superior atria is predominantly circumferential (with respect to the *Z*-axis) and is more vertical inferiorly (see Figure 2). The most prominent fiber tracts—CT, PM, and BB—are consistent with previous descriptions of these structures.[7,8] Of note are the bifurcations in the BB with minor branches tracking downward adjacent to the RAA and the LAA (see Figure 2A and 3F). Furthermore,

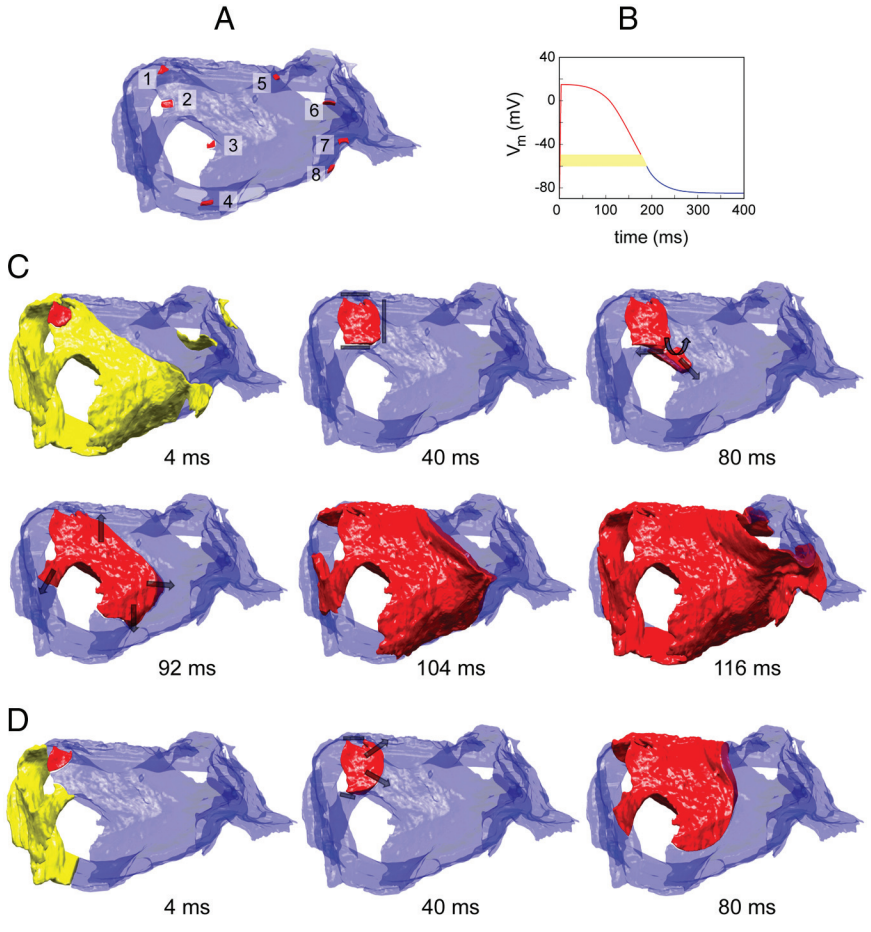

Figure 8. Comparison of effects of anisotropic and isotropic electric properties on epicardial spread of ectopic electric activation in the posterior left atrium (PLA) induced with the following S_1-S_2 stimulation protocol. The S_1 stimulus is "normal" sinoatrial node pacing, as shown in Figure 5. S_2 stimuli were applied at the 8 locations in **A**, when membrane potential (V_m) due to the S_1 stimulus repolarized to −50 mV and −55 mV for anisotropic and isotropic electric properties, respectively. Potentials are color-coded, as displayed in **B**, for anisotropic case. Time course of activation in PLA after S_2 stimulus was delivered at location **1** for **C**, anisotropic, and **D**, isotropic properties.

in the upper anterior LA, the BB appears to blend with circumferential myofibers in the inner half of the wall (see Figure 2A and online-only Data Supplement Figure IV, C). Ho et al[7] described other characteristic myofiber organization in the interatrial septum and LA, including the SPB and septo-atrial bundle. Although it is difficult to replicate the curvilinear viewing planes used in their dissections, the regions of uniformly organized myofibers reported—fibers in or near parallel to the transverse plane in the anterior LA roof, the longitudinal orientation of fibers in the septum and LA wall adjacent to it, and finally, the transverse orientation of subendocardial fibers toward the base of the LA—all appear to be consistent with these earlier descriptions. These findings confirm that the principal features of atrial myoarchitecture are conserved in large mammalian hearts despite differences within and between species.

It is to be expected that our work should be consistent with previous anatomic descriptions.[7,8] The myofibers tracked visually in dissected fixed hearts are bundles of myocytes, and the structure tensor analysis applied here identifies the cleavage planes between these bundles. There is some potential for error with this approach: (1) thick bands of connective tissue at the atrial surfaces and surrounding blood vessels may generate artifact; (2) variations in staining between serial sections gives rise to scatter and may introduce some bias; and (3) voxel resolution in the image volume analyzed is only $50\times50\times50$ μm^3. We have refined our image processing procedures to minimize the effects of these factors. Additionally, each of our serial sections was imaged at 8×8-μm^2 resolution, which means that individual myocytes could be identified and orientations checked visually. This was done systematically as a means of internal validation. The main difference between this and earlier anatomic studies is that we have generated comprehensive, quantitative data on atrial myofiber architecture not previously available.

Effects of Atrial Myofiber Architecture on Electric Activation

We used our structurally detailed model of atrial anatomy to investigate the effects of myofiber architecture on atrial electric activation. This was done by comparing the spread of electric activation with anisotropic and isotropic electric properties, using a Fenton-Karma activation model[13] adapted to provide an accurate representation of phase 0 of the atrial action potential (see online-only Data Supplement). We opted for anisotropic electric properties that produce very similar regional activation spread to those seen with isotropic properties in the absence of ordered myofiber organization (see online-only Data Supplement Figure V).

Comparison of activation spread modeled with isotropic and anisotropic electric properties (see Figure 5) demonstrates the impact of myofiber tracts throughout the atria. Activation spreads more rapidly across the endocardial surface of the RA in the anisotropic case, reflecting rapid propagation through the CT and PM (see Figure 5). However, the greatest differences are seen in the LA, with accelerated spread from right to left across the upper anterior atria via the BB and fiber tracts adjacent to it. Most striking is the time course of electric activation in the PLA, where the ordered arrangement of myocytes in the interatrial septum and LA generate preferential propagation from anterior to posterior sides of the LA between right and left PVs (see Figure 7). This gives rise to marked activation time dispersion adjacent to the left PVs.

The activation spread predicted here on the basis of myofiber architecture corresponds very closely to atrial activation patterns mapped in humans,[17] dogs,[18,19] and sheep[20–22] in sinus rhythm or during electric stimulation adjacent to the SAN. In particular, the model replicates normal propagation through the anterior and posterior LA walls during sinus rhythm or stimulation adjacent to the SAN with final activation adjacent to the left inferior PV observed in humans[17] and dogs.[18,19] It also reproduces the anisotropic spread of electric activation across the PLA in sinus rhythm in the sheep.[22]

Over the past decade, it has become evident that the muscular architecture and electric properties of the PLA and PVs play a crucial role in the initiation and maintenance of AF.[22,23] For ectopic electric activity originating in the PV sleeves, the abrupt changes in myofiber orientation and wall thickness at the junctions of the PVs and LA are thought to give rise to conduction delays and block as a result of current-load mismatch, providing a substrate for reentry.[22,23] The present study confirms the complexity of myofiber architecture and geometry adjacent to the PV ostia but suggests that the mechanisms responsible for block and slow propagation in the PLA may be more complex than previously thought.

We mimicked the effects of ectopic activity at the PV sleeves by applying S_2 stimuli at the PV junctions at the start of the vulnerable period after S_1 activation from the SAN (see Figure 8 and online-only Data Supplement Figure VII). Successful propagation occurred at shorter coupling intervals with anisotropic electric properties than with isotropic properties but was slow and highly directional. With anisotropic electric properties, transverse current flow is decreased. This reduces current load, enabling propagation to occur earlier in the relative refractory period; however, conduction blocks transverse to the myocyte axis.[6]

These considerations explain the nonuniform initial spread of electric activation from the S_2 stimulus site in Figure 8C. Activation spreads first along the PV sleeve, but, with the abrupt rotation of myofiber orientation at the PV junction, propagation across the LA roof is blocked and follows the muscle fibers that wrap circumferentially around the left PVs. The slow spread of activation, in this case, during the first 80 ms after S_2 stimulation, is explained in part by the marked repolarization gradients across the inferolateral PLA (Figure 8C, 4 ms). Preferential propagation around the medial side of the left PVs directs activation toward a region of the PLA, where repolarization and CV restitution are initially incomplete. The repolarization gradients reflect the dispersion of activation times in the PLA (see Figure 7), which, as discussed previously, is a result of the complex myofiber pathways adjacent to the BB, around the PVs, and between the PVs (the SPB). In summary, the results of these numeric experiments are consistent with previous views[22,23] that the complex myofiber architecture at the junction of PLA and PVs provides a substrate for reentry. However, they suggest

that repolarization time dispersion adjacent to the PVs, which results from the organization of myofiber bundles in the PLA, also plays a role in the initiation of reentrant arrhythmia.

We used spatially uniform isotropic and anisotropic electric properties to model electric activation because it is the most direct way of demonstrating the qualitative effects of atrial myofiber architecture on this process. The electric properties selected gave rise to CVs ≈1.13 m/s in the fiber direction and ≈0.63 m/s transverse for the anisotropic case in regions where myofibers were uniformly aligned. In the absence of ordered myofiber organization, CV was ≈0.75 m/s in all directions, very similar to that observed throughout the atria with isotropic electric properties. Although these CVs lie within the range measured in atrial tissues,[2] electric properties are not spatially uniform even in the normal atria. We probably have overstated the extent of electric anisotropy in working atrial myocardium and understated axial CVs for specialized myofiber tracts such as the BB and CT (see the online-only Data Supplement). This is consistent with the fact that predicted total activation times are somewhat longer than those observed experimentally in the normal atria.[21,22] Spatial nonuniformity of atrial electric properties is exacerbated by the structural and electric remodeling that occurs with ageing and many forms of heart disease, and this is thought to increase the risk of atrial rhythm disturbance. For instance, we have demonstrated that abrupt changes in geometry and myofiber orientation at the junction of PV sleeves and PLA give rise slow propagation and activation delays with ectopic activation from the PV sleeves. Almost certainly, heterogeneous atrial electric properties amplify the probability that these factors will give rise to wave break and reentry in patients that are prone to AF.

Future Work

We believe that image-based computer models provide an important platform for better understanding the mechanisms responsible for initiation and maintenance of AF. However, the corollary to this is that the structural remodeling and the spatial variation of atrial electric properties that occur with ageing and heart disease must be incorporated into such models to enable comprehensive analyses of rhythm disturbance to be undertaken. These issues are being addressed in research currently being carried out in our laboratories. The data presented are for the normal sheep heart. Comparable information is being acquired for a sheep heart failure model. These structural data sets will be made available to other researchers via the repository operated by the Cardiac Atlas Project (http:www.cardiacatlas.org).

Conclusions

In this study, we have (1) developed novel techniques that enable surface geometry and myofiber architecture to be characterized throughout the atrial chambers and (2) modeled the spread of electric activation on this structure. We have shown that preferential electric conduction in the atria reflects ordered myocyte arrangement over length scales on the order of millimeters and have confirmed the effects of specialized myofiber tracts such as the CT, PMs, and the BB on the spread of activation from the SAN. We have demonstrated quantitatively, for the first time as far as we are aware, how the arrangement of myocyte bundles such as the BB and the SPB contributes to activation time dispersion in the PLA. Finally, our analysis of structural mechanisms that contribute to increased vulnerability to ectopic stimuli originating from the PV sleeves shows that image-based computer models provide a powerful platform for investigating arrhythmic substrates in the atria.

Acknowledgments

We are sad to note that our coauthor and valued colleague, Professor Andrew J. Pullan, died on March 7, 2012, at age 48. We thank Dr Rita Yassi for her perseverance and skill in acquiring the atrial serial images and Dane Gerneke for his expert technical support.

Sources of Funding

This work was supported by the Health Research Council of New Zealand, the British Heart Foundation, the Wellcome Trust, and the Engineering and Physical Sciences Research Council of the United Kingdom.

Disclosures

None.

References

1. Schotten U, Verheule S, Kirchhof P, Goette A. Pathophysiological mechanisms of atrial fibrillation: a translational appraisal. *Physiol Rev*. 2011; 91:265–325.
2. Harrild DM, Henriquez CS. A computer model of normal conduction in the human atria. *Circ Res*. 2000;87:25–36.
3. Virag N, Jacquemet V, Henriquez CS, Zozor S, Blanc O, Vesin JM, Pruvot E, Kappenberger L. Study of atrial arrhythmias in a computer model based on MR images of human atria. *Chaos*. 2002;12:754–763.
4. Seemann G, Höper C, Sachse FB, Dössel O, Holden AV, Zhang HG. Heterogeneous three-dimensional anatomical and electrophysiological model of human atria. *Phil Trans R Soc A*. 2006;364:1465–1481.
5. Aslanidi O, Boyett M, Li J, Dobrzynski H, Zhang H. Mechanisms of transition from normal to reentrant electrical activity in a model of rabbit atrial tissue: interaction of tissue heterogeneity and anisotropy. *Biophys J*. 2009;96:798–817.
6. Zhao J, Trew M, LeGrice I, Smaill B, Pullan A. A tissue-specific model of reentry in the right atrial appendage. *J Cardiovasc Electrophysiol*. 2009;20:675–684.
7. Wang K, Ho SY, Gibson DG, Anderson RH. Architecture of atrial musculature in humans. *Heart*. 1995;73:559–565.
8. Ho SY, Sánchez-Quintana D. The importance of atrial structure and fibers. *Clin Anat*. 2009;2:52–63.
9. Dobrzynski H, Li J, Tellez J, Greener ID, Nikolski VP, Wright SE, Parson SH, Jones SA, Lancaster MK, Yamamoto M, Honjo H, Takagishi Y, Kodama I, Efimov IR, Billeter R, Boyett MR. Computer three-dimensional reconstruction of the sinoatrial node. *Circulation*. 2005;111: 846–854.
10. Li J, Greener ID, Inada S, Nikolski VP, Yamamoto M, Hancox JC, Zhang H, Billeter R, Efimov IR, Dobrzynski H, and Boyett MR. Computer three-dimensional reconstruction of the atrioventricular node. *Circ Res*. 2008;102:975–985.
11. Streeter DD, Spotnitz HM, Patel DP, Ross J, Sonnenblick EH. Fiber orientation in the canine left ventricle during diastole and systole. *Circ Res*. 1969;24:339–347.
12. Helm PA, Tseng HJ, Younes L, McVeigh ER, Winslow RL. Ex vivo 3D diffusion tensor imaging and quantification of cardiac laminar structure. *Magn Reson Med*. 2005;54:850–859.
13. Fenton F, Karma A. Vortex dynamics in three-dimensional continuous myocardium with fiber rotation: filament instability and fibrillation. *Chaos*. 1998;8:20–47.
14. Moe GK, Rheinboldt WC, Abildskov JA. A computer model of atrial fibrillation. *Am Heart J*. 1964;67:200–220.

15. Vigmond EJ, Ruckdeschel R, Trayanova NA. Reentry in a morphologically realistic atrial model. *J Cardiovasc Electrophysiol*. 2001;12: 1046–1054.
16. Krause M, Hausherr JM, Burgeth B, Herrmann C, Krenkel W. Determination of the fibre orientation in composites using the structure tensor and local X-ray transform. *J Mater Sci*. 2010;45:888–896.
17. De Ponti R, Ho SY, Salerno-Uriarte JA, Tritto M, Spadacini G. Electroanatomic analysis of sinus impulse propagation in normal human atria. *J Cardiovasc Electrophysiol*. 2002;13:1–10.
18. Sakamoto S-I, Nitta T, Ishii Y, Miyagi Y, Ohmori H, Shimizu K. Interatrial electrical connections: the precise location and preferential conduction. *J Cardiovasc Electrophysiol*. 2005;16:1077–1086.
19. Hayashi H, Lux R, Wyatt R, Burgess MJ, Abildskov JA. Relation of canine atrial activation sequence to anatomic landmarks. *Am J Physiol Heart Circ Physiol*. 1982;242:421–428.
20. Gray RA, Pertsov AM, Jalife J. Incomplete reentry and epicardial breakthrough patterns during atrial fibrillation in the sheep heart. *Circulation*. 1996;94:2649–2661.
21. Berenfeld O, Zaitsev AV. The muscular network of the sheep right atrium and frequency-dependent breakdown of wave propagation. *Anat Rec*. 2004;280:1053–1061.
22. Klos M, Calvo D, Yamazaki M, Zlochiver S, Mironov S, Cabrera J-A, Sanchez-Quintana D, Jalife J, Berenfeld O, Kalifa J. Atrial septopulmonary bundle of the posterior left atrium provides a substrate for atrial fibrillation initiation in a model of vagally mediated pulmonary vein tachycardia of the structurally normal heart. *Circ Arrhythmia Electrophysiol*. 2008;1:175–183.
23. Hocini M, Ho SY, Kawara T, Linnenbank AC, Potse M, Shah D, Jais P, Janse MJ, Haissaguerre M, de Bakker JMT. Electrical conduction in canine pulmonary veins: electrophysiological and anatomic correlation. *Circulation*. 2002;105:2442–2448.

CLINICAL PERSPECTIVE

Atrial fibrillation (AF) is the most common heart rhythm disturbance, and it is associated with significant morbidity and mortality. The role of the pulmonary veins (PVs) in triggering AF is well established, but the mechanisms by which atrial myofiber architecture contributes to reentry are less clear. To address this issue, we quantified chamber geometry and myofiber orientations throughout the normal atria for the first time and incorporated these data into a 3D computer model of atrial electric activation. We show that specialized conduction tracts and myofiber bundles in septum and posterior left atrium (PLA) give rise to marked activation time dispersion adjacent to the PV junctions in sinus rhythm. We have also demonstrated slow propagation and activation delays when ectopic PV stimuli follow sinus activation. Contributing factors include the abrupt changes in geometry and myofiber orientation at the veno-atrial junctions as well as activation time dispersion in the PLA. The heterogeneous atrial electric properties associated with ageing and structural heart disease almost certainly amplify the probability that these factors will give rise to wave break and reentry. We conclude that anatomically realistic, image-based computer models offer a potentially powerful platform for investigating mechanisms that underlie the initiation and maintenance of reentrant atrial arrhythmias.